The Effects of Geometric Parameters Under Small and Large Deformations on Dissipative Performance of Shape Memory Alloy Helical Springs

Y. Mohammad Hashemi, M. Kadkhodaei*

Department of Mechanical Engineering, Isfahan University of Technology, Isfahan, Iran.

Article info

Abstract

This paper presents an investigation into shape memory alloy (SMA) springs considering the effects of geometry changes under small as well as large deformations. Helical springs were fabricated by shape setting of NiTi wires through heat treatment. The products exhibited pseudoelasticity at the ambient temperature, and their force-displacement responses were examined by performing simple tension tests. A model was further proposed to study tension and compression of SMA springs, and it was shown that the consequences of geometrical changes in tension and compression of springs are different. The numerical results of large and small deformation models were verified by experimental tensile results. In order to design a spring with maximum dissipative performance, a designer has three geometric parameters to set: wire diameter, spring diameter, and the number of active coils. The influences of these parameters on dissipated energy were studied in both displacement- and force-control loadings, and a framework for designing SMA springs with the purpose of achieving maximum applicable dissipation was at last developed.

Nomenclature

Notation			
A_f	Austenite final temperature	A_s	Austenite start temperature
C_{Af}	Finish slope of the reverse transformation strip	C_{As}	Start slope of the reverse transformation strip
C_{Mf}	Finish slope of the forward transformation strip	C_{Ms}	Start slope of the forward transformation strip
d	Wire diameter of the helical spring	D	Diameter of the helical spring
D_0	Initial diameter of the helical spring	E	Young's modulus of SMA
E_A	Austenite Young's modulus	E_M	Martensite Young's modulus
F	Axial force	G	Shear modulus of SMA
G_A	Austenite shear modulus	G_M	Martensite shear modulus
L	The length of wire that spring has been fabricated from	r	Radial coordinate along the wire cross-section
M_s	Martensite start temperature	N	Number of active coils

*Corresponding author: M. Kadkhodaei (Professor)
E-mail address: kadkhodaei@cc.iut.ac.ir

Nomenclature

Notation			
M_f	Martensite final temperature	R_f	R-phase final temperature
R_s	R-phase start temperature	T	Temperature
T'	Torque		
Greek Letters			
α	Helix angle	α_0	Initial helix angle
γ	Shear strain	γ^*	Maximum recoverable shear strain
γ^{tr}	Transformation shear strain	δ	Displacement
ϵ	Total strain	ϵ^*	Maximum recoverable strain
ϵ^e	Elastic strain		

1. Introduction

Shape memory alloys (SMAs) are a category of smart materials that have been used in various fields over the past decades. Due to having two main extraordinary responses of shape memory effect (SME) and pseudoelasticity, they are used in manufacturing actuators, sensors, hybrid composites, coupling, fasteners, and damping systems [1, 2]. They are also employed in self-healing materials owing to the crack closure effect [3]. Different geometries of shape memory alloys such as wire, spring, and tube are available on the market. Although wire is, by far, the most usable geometry, it is not able to appropriately resist compression. SMA springs, unlike SMA wires, are capable of tolerating compression. They are also able to withstand elongations as large as 1250% [4]. SMA springs have been employed in a wide range of applications, including sensors, actuators, and passive as well as active isolators (especially in the civil engineering context) [2, 5].

Zhuang et al. [6] employed a sliding-type bearing using SMA springs for seismic protection systems and studied the proposed prototype by experiments as well as numerical simulations. An excellent energy dissipation capacity was also observed from the employed prototype [6]. Attanasi et al. [7] investigated the compressive and tensile response of SMA springs experimentally. A numerical analysis was performed applying a finite element model and found asymmetric response of an SMA spring under tensile and compressive loadings [7]. Attanasi et al. [7] also observed buckling in their numerical and experiment results. An SMA spring experiences geometric changes upon large amounts of applied displacements, which can considerably affect the force-displacement response of spring. Some efforts were made to simulate the mechanical response of SMA springs in large deformations; as Savi et al. [8] reported that the larger geometric nonlinear effects are associated with larger spring index values. They employed finite element method and studied large deformation effects in springs with different geometries [8]. Wang et al. [9] proposed a thermomechanical coupled finite deformation model for SMAs, and implemented their model into ABAQUS to predict the mechanical

as well as thermal response of SMA springs. Due to some challenges including computational costs of employing FEM, it has been a tendency towards proposing simple models so some efforts have been made to present a 1D model considering large deformation effects [10, 11]. An et al. [10] proposed an explicit correlation for the calculation of applied force (in the case of displacement-control loadings) using some simplification assumptions, which do not necessarily coincide with the reality. As a matter of fact, since every point in the cross-section of an SMA spring experiences a different response, there cannot be an explicit formulation for the calculation of force as a function of deflection. Although the force-displacement response of a pseudoelastic spring can be predicted by straightforward hysteresis models, like Preisach approach, these models are not able to consider the effects of material and geometrical parameters on the predicted results [12]. Heidari et al. [13] studied the response of SMA springs neglecting large deformation effects. They verified their numerical results with experimental findings under quasi-static conditions, and good agreements were reported between experiments and numerical findings [13].

One of the most important applications of pseudoelastic springs is in seismic and isolation systems. In such applications, an SMA spring is simultaneously serving as an absorbing and dissipating component. Dissipative performance of an SMA spring depends on the material parameters, ambient temperature, loading conditions, and of course the spring geometry. For the purpose of designing an SMA spring with desired dissipation energy, a designer has three geometric parameters to set: wire diameter (d), spring diameter (D), and the number of active coils (N). Proposing a design framework for the purpose of optimizing the dissipative energy of SMA springs is a crucial issue to which less attention has been paid so far.

The present work aims to propose a 1D numerical model for SMA springs considering the effects of large deformation through developing Heidari's model [13]. Unlike Heidari's formulation, the current model is capable of predicting the force-displacement response of SMA springs under large amounts of displacement, ow-

ing to the consideration of spring diameter variations as well as initial helix angle in loading and unloading. Required experimental samples were fabricated and quasi-static tensile tests were conducted. Numerical results were verified by comparing them with the experimental findings. The influence of spring geometry on the dissipative performance was studied under displacement- and force-control loadings, and a guideline for geometry design process is presented in the results section.

2. Experiments

Heidari et al. [13] investigated the fabrication process of SMA springs showing SME at the ambient temperature. Jahanbazi et al. [14] studied the effects of cooling rate, cold work, temperature, and duration time of heat treatment on the transformation temperatures of fabricated SMA springs. They also presented a guideline for fabricating SMA springs exhibiting a desired response at the ambient temperature. Founded on these findings, NiTi SMA wire showing pseudoelastic response at the ambient temperature was used for the fabrication of SMA springs. At first, the wire was wound around a dedicated screw and constrained by side nuts. The set was then placed inside the furnace which was stabled at 750°C. The furnace was turned off after ten minutes, and 270 minutes were given to the whole system for cooling to the ambient temperature. The employed instruction for fabricating an SMA spring showing the pseudoelastic response at the room temperature was used from Jahanbazi's investigation [14]. Fig. 1 shows a fabricated spring. Tensile tests were accomplished on three fabricated springs using a SANTAM STM-50 simple testing machine at the ambient temperature and also elevated temperatures with the speed of 1mm/min. The repeatability of the fabricating process was verified by comparing the tensile responses of three specimens at the ambiant temperature. Fig. 2 demonstrates the response of specimens at three temperatures of 43, 59, and 68°C. It is noticeable that the specimens showed pseudoelastic response at temperatures higher than 16°C.
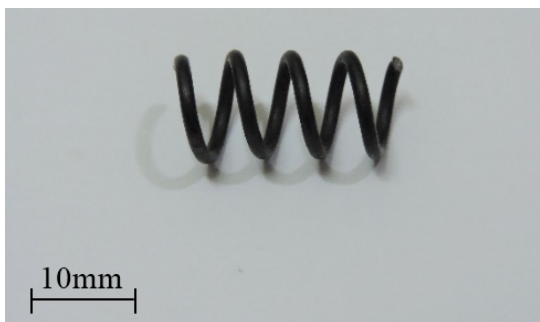

Fig. 1. Fabricated SMA spring exhibiting pseudoelastic response at the ambient temperature.
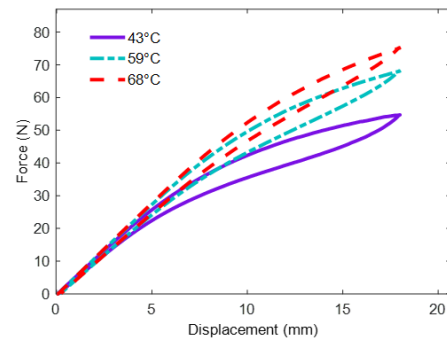

Fig. 2. Force-displacement response of the fabricated springs at different temperatures.

3. Modeling

The total strain of an SMA wire can be expressed as decompositions of elastic (ϵ^e) and transformation (ϵ^{tr}) components [15]. The transformation strain can be written as Eq. (3):

$$\epsilon = \epsilon^e + \epsilon^{tr} \tag{1}$$

$$\epsilon^e = \frac{\sigma}{E} \tag{2}$$

$$\epsilon^{tr} = \epsilon^* \xi_s \tag{3}$$

In which ϵ^*, E, σ, and ξ_s represent maximum recoverable strain, the Young's modulus, stress, and stress-induced martensite volume fraction, respectively. Young's modulus is a function of martensite volume fraction and can be written as:

$$\frac{1}{E} = \frac{\xi}{E_M} + \frac{1-\xi}{E_A} \tag{4}$$

$$\xi = \xi_s + \xi_t \tag{5}$$

where E_M, E_A, ξ_t, and ξ represent Young's modulus of pure martensite, Young's modulus of pure austenite, temperature-induced martensite volume fraction, and martensite volume fraction, respectively. Martensite volume fraction can be calculated through the correlations proposed by Brinson and Chung [15, 16].

Heidari et al. [13] generalized Brinson's model for shear loading by engaging von-Mises equivalent stress and strain:

$$\gamma = \gamma^{tr} + \frac{\tau}{G} \tag{6}$$

$$\gamma^{tr} = \gamma^* \xi_s(\sigma_{eq}) = \gamma^* \xi_s(\tau\sqrt{3}) \tag{7}$$

$$\gamma = \frac{\tau}{G(\xi)} + \gamma^* \xi_s(T, \tau\sqrt{3}) \tag{8}$$

in which γ, γ^{tr}, σ_{eq}, τ, T, G, and γ^* are the total shear strain, transformation shear strain, von-Mises equivalent stress, shear stress, temperature, elastic shear

modulus, and maximum recoverable shear strain, respectively. The axially-applied force on the spring can be calculated by Eqs. (9) and (10) [13]:

$$F = \frac{4\pi}{D} \int_0^{\frac{d}{2}} \tau r^2 dr \qquad (9)$$

$$F\frac{D}{2} = T' \qquad (10)$$

in which F, T', D, d, and r represent applied force, torque, the spring diameter, the wire diameter and radial coordinate in spring cross-section, respectively. Heidari et al. [13] neglected the geometric nonlinearities and considered a constant value for spring diameter. However, some crucial geometry changes happen in a spring undergoing a large amount of deflection. Variations in the spring geometry under tension differ from what happens in compression. For instance, in tension, the spring diameter decreases with increase in the amount of applied deflection; but, in compression, the spring diameter increases as deflection increases. Wahl et al. [17] proposed Eq. (11) which considers the effect of initial helix angle. By tracing the helix angle of a spring in different stages of loading, the associated spring diameter can be calculated by Eqs. (12) and (13).

$$\gamma(\alpha) = \frac{d}{D_0} \cos\alpha_0 (\sin\alpha - \sin\alpha_0) = \frac{d}{D_0}\frac{\delta}{L}\cos\alpha_0 \quad (11)$$

$$\delta = L(\sin\alpha - \sin\alpha_0) \qquad (12)$$

$$\frac{D}{D_0} = \frac{\cos\alpha}{\cos\alpha_0} \qquad (13)$$

where D_0, α_0, α, L, and δ represent initial spring diameter, initial helix angle, helix angle, the length of wire that spring has been fabricated from, and applied displacement, respectively. Modeling the mechanical response of SMA springs considering large deformation effects was performed by applying Eqs. (11-13)

into Heidari's model using programming in MATLAB. The numerical calculations started with defining required integral points at the spring cross-section. By incrementally increasing the applied displacement, the shear strain was calculated for integral points using large deformation correlations, and consequently the shear stress distribution at the spring cross-section was obtained by employing the constitutive equation. The value of axially applied force to the spring was calculated by shear stress distribution at the spring cross-section. Since some material parameters of fabricated springs, such as transformation temperatures, differ from those of the straight wire, a set of material parameters associated with the fabricated springs is needed.

The transformation temperatures were obtained from differential scanning calorimetry (DSC) test and are listed in Table 1. R_s and R_f are the R-phase start and finish temperatures respectively. The phase diagram of the specimens is shown in Fig. 3, where different slopes for martensite and austenite strips are considered [18, 19]. The material and geometrical parameters associated with fabricated springs are listed in Table 2. M_s, M_f, A_s, A_f, σ_s^{cr}, and σ_f^{cr} represent the start and finish temperatures of martensite transformation, the start and finish temperatures of austenite transformation, the start and finish stresses of detwinning, respectively. Also, C_{Ms}, C_{Mf}, C_{As}, and C_{Af} are the shown slopes in Fig. 3. C_{Ms} and C_{Af} were obtained from experimental results of Fig. 2 by calculating the start stresses of forward transformation and finish stresses of backward transformation at different temperatures. Since all material parameters of SMA springs, including σ_s^{cr}, σ_f^{cr}, and ϵ^* cannot be determined by experimental tensile test, the values of these parameters were obtained for the raw wire by conducting tensile tests, and they were extended to SMA springs. However, E_A and E_M were determined by slopes of force-displacement responses of specimens at the primary stages of loading as well as unloading cycles.

Table 1
Transformation temperatures of the specimens.

R_s(°C)	R_f(°C)	A_f(°C)	A_s(°C)	R_s(°C)	R_f(°C)	M_s(°C)	M_f(°C)
-7	4	16	7	22	-6	-37	-

Table 2
Material and geometrical parameters of the fabricated springs.

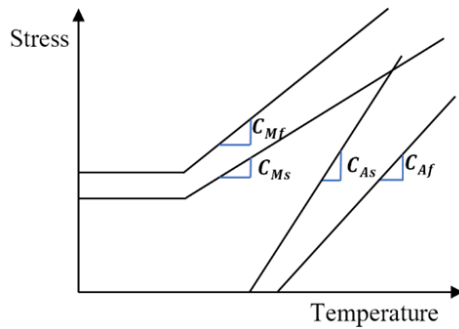| E_A(GPa)	E_M(GPa)	σ_s^{cr}(MPa)	σ_f^{cr}(MPa)
39.6	20	20	80
A_f(°C)	A_s(°C)	M_s(°C)	M_f(°C)
16	7	-37	-
C_{Ms}(MPa/K)	C_{Mf}(MPa/K)	C_{As}(MPa/K)	C_{Af}(MPa/K)
3.9	7.3	15	7.8
ϵ^*	d(mm)	D(mm)	N
0.057	1.5	8.6	3

Fig. 3. Phase diagram.

4. Results and Discussion

The characterized material parameters of fabricated springs were imported into large and small deformation models, and the numerical results were compared with experimental findings. Fig. 4 shows these observations at the ambient temperature of 27°C. There is an error of 7% in force prediction through small deformation model at the given displacement of 18mm, and it is reduced to 2% by considering the geometrical effects of large deformation. The reason of selecting final displacement for the error calculations is to prevent the errors of neglecting R-Phase (rhombohedral) and large deformation effects to be combined. In other words, the authors believe that the difference between experiment and predicted values of force in displacements in the range of 5-10mm is caused by R-Phase, and it is reduced at larger displacements. With respect to Fig. 4 and the trends of illustrated curves, error in predicting the applied force through small deformation model increases by increasing the amount of applied displacement and, as is expected, it is more crucial to consider large deformation effects when large amounts of displacement appear in the spring.

Since the material parameters given in Table 2 were reported for an SMA associated to a phase diagram with different slopes for start and finish lines of stress, another empirical set of material parameters with the same slopes for start and finish lines were employed for the rest of study (Table 3). This prevents from combining different effects on the results and helps the influences of each individual parameter to be distinguishable. A spring with an index of 6 and five active coils was considered for the case study, and numerical results were obtained at 72°C. By taking a closer look at Fig. 5, it can be found that unlike loading, in unloading, outer ring at the spring cross-section is not the region from which transformation from martensite to austenite starts. In other words, in loading, transformation starts from the outer ring at the spring cross-section and propagates to the central point; but, in unloading, the transformation initiates from somewhere near the outer ring and bilaterally spreads (Fig. 5b).
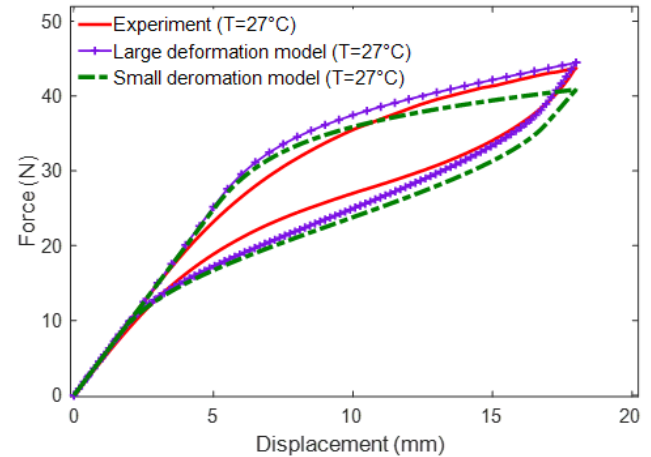

Fig. 4. Comparison between small and large deformation models with experiment at 27°C.

The effects of large deformation in helical springs are not necessarily negligible under either tensile or compressive loadings. However, unlike compression, increase in helix angle under tension causes the spring diameter to decrease. On the other hand, according to Eq. (11), in springs with small initial helix angle, the impact of initial helix angle on the shear strain is negligible. Thus, as is shown in Fig. 6a, at the early stages of tensile loadings, the response of an SMA spring can be predicted employing small deformation model; however, by increasing the amount of applied displacement, small deformation model predicts the force with a considerable error of 27% (at 97mm deflection). Compression springs generally have larger initial helix angles in comparison to tensile ones. Thus, according to Eq. (11), due to the impact of initial helix angle on the shear strain, in compressive springs, small deformation model predicts the response with a remarkable error even at the early stages of loading (Fig. 6b). The spring diameter increases with decrease in helix angle and, unlike tension, there is a gentle growth in force response for compressive springs. Fig. 6c reveals that the current model is also able to be employed for the shape memory effect (SME).

Table 3
Material and geometrical parameters employed for generating figures 5-14.

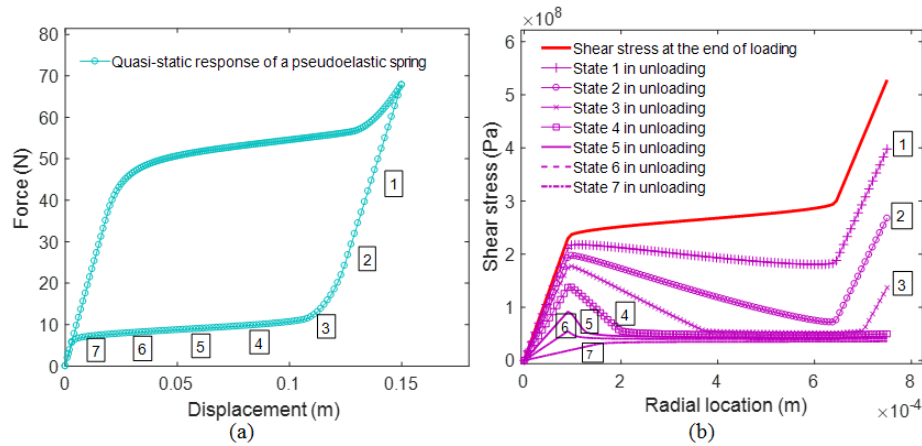| G_A(MPa)	G_M(MPa)	M_f(K)	M_s(K)	A_s(K)	A_f(K)	C_M(MPa/K)
10797	9210	274.5	289.9	322.2	332.6	7.23
C_A(MPa/K)	σ_s^{cr}(MPa)	σ_f^{cr}(MPa)	ε^*	N	D(mm)	d(mm)
4.3	5	116	0.069	5	9	1.5

Fig. 5. (a) Force-displacement response and (b) Stress distribution at the cross-section of a pseudoelastic tensile spring under loading and unloading at 72°C.
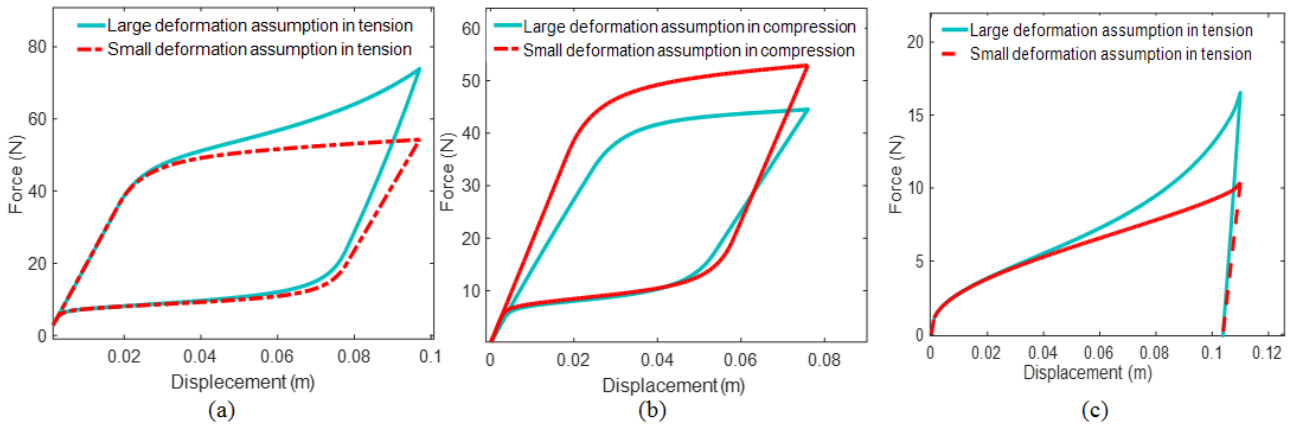

Fig. 6. Comparison between small and large deformation models for: (a) The tensile pseudoelastic response, (b) The compressive pseudoelastic response of an SMA spring with initial length of 84 mm, (c) Tensile SME response of an SMA spring at 17°C.

Table 4
Geometrical parameters used for generating Figs. 7-12.

Force-control				Displacement-control			
D(mm)	d(mm)	N	F_f(N)	D(mm)	d(mm)	N	δ_f(cm)
9-15	1.5	5	90	9-15	1.5	5	12
15	1.5-2.5	5	120	15	1.5-2.5	5	21
15	1.5	5-10	40	15	1.5	5-10	20

Due to the importance of dissipated energy of an SMA spring in applications such as seismic devices and isolators, further investigation was performed on the effect of spring geometry on the dissipated energy of tensile springs. It is notable to mention that, in order to design an SMA spring with high dissipative performance, it is more straightforward for a designer to optimize the geometry than to change the type of the employed wire; because modeling a SMA spring fabricated by a different type of wire requires repeating the characterization of material parameters, which is a time consuming and expensive process. Since a designer needs to choose one condition between displacement- and force-control for designing the geometry, these two conditions were here investigated by employing large deformation model for different geometries according to the details provided in Table 4. Being force- or displacement-control of a spring refers to the application. For example, an employed spring in a mass isolation system, with constant mass and unlimited displacement, operates in force-control condition. While, by limiting the final applied displacement, the operational condition of the spring is converted to displacement-control.

Figs. 7-12 show the effect of spring geometry on the force-displacement response as well as dissipated energy at 345K. As illustrated in Fig. 7a, increase in spring diameter under displacement-control loadings

causes a reduction in stiffness. Due to the final displacement limitation and the significant drop in force values, dissipated energy decreases (Fig. 8a). In the force-control condition, the effect of decrease in force values is compensated by the growth in displacement values (Fig. 7b). This phenomenon leads to a bell-shaped dissipative response as is demonstrated in Fig 8b. In other words, change in the ascending trend to the descending one in Fig. 8b is caused by considerably decrease in force values.

According to Eq. (11), in limited final displacement conditions, shear strain increases with an increase in wire diameter. Consequently, under displacement-control loadings, springs with a large wire diameter experience the transformation sooner than springs with small ones. As can be seen in Figs. 9a and 10a, the response of dissipative performance under displacement-control loadings is ascending. Although under force-control loadings, the force values increase by increasing the wire diameter, at a given final force limitation, the transformation is postponed and dissipation energy drops significantly (Figs. 9b and 10b). It is notable that the spring index increases by decreasing wire diameter and, as shown in Fig. 9, springs with a higher index show more nonlinearity in their response. In particular, by comparing the force-displacement response of springs with wire diameter of 1.5 and 2.25mm in Fig. 9b, it can be concluded that, unlike the spring with

2.25mm wire diameter, for the spring with 1.5mm wire diameter the force-displacement response is nonlinear even in the course of unloading when transformation has not started yet.

The most convenient way to optimize dissipative performance by altering one geometry parameter is to change the number of active coils. Figs. 11a and 12a show the effect of the number of active coils on force-displacement response as well as dissipation of an SMA spring under displacement-control loading. Springs with a smaller number of active coils have larger stiffness values; thus, force levels in loading path increase by decreasing the number of active coils. According to Fig. 11a, for the displacement range between 0.08m and 0.16m, unlike loading, although force values increase by increasing the number of active coils in unloading path, due to the larger values of force in loading, loading path has a more powerful effect on the trend of dissipated energy (Fig. 12a). Since, under force-control loadings, change in the number of active coils does not affect stress distribution within the spring cross-section, applied force on each coil remains constant, so the number of active coils has a linear influence on dissipation (Figs. 11b and 12b). In other words, Fig. 11b illustrates that force-displacement response is just scaled in displacement axis by varying the number of active coils.
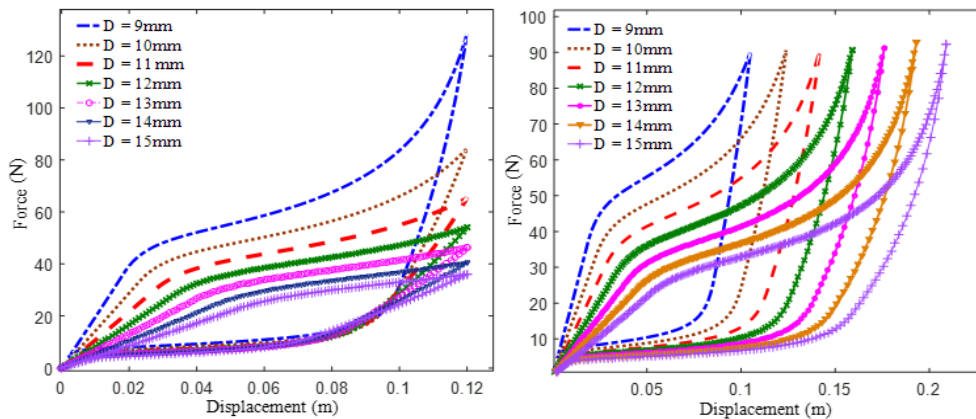

Fig. 7. The effect of spring diameter on force-displacement response of an SMA spring under: (a) Displacement-control and loading (b) Force-control loading.
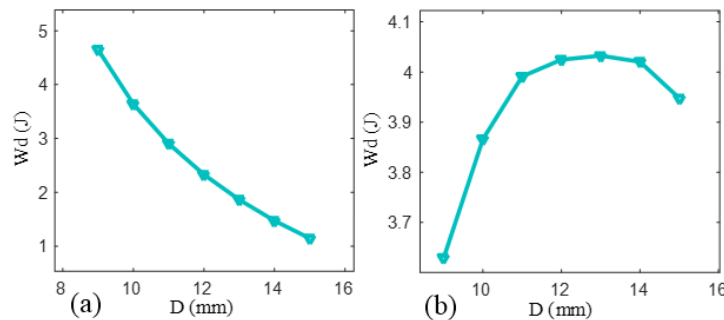

Fig. 8. The effect of spring diameter on energy dissipation under: (a) Displacement-control loading, (b) Force-control loading.
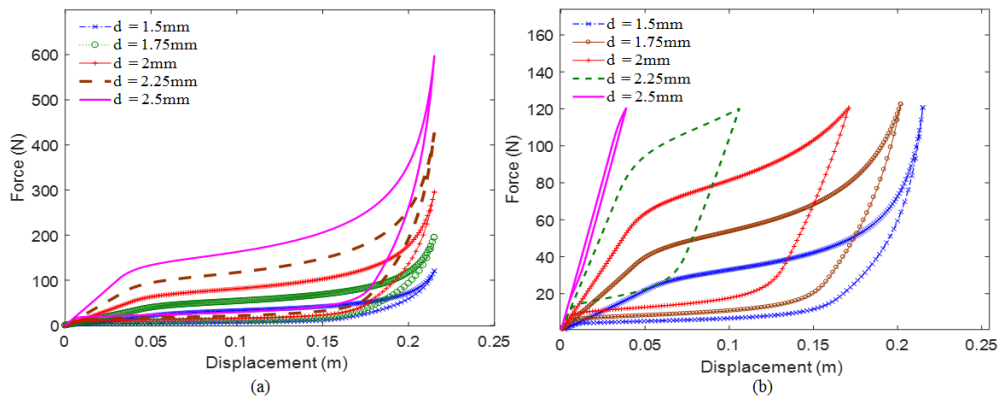
Fig. 9. The effect of wire diameter on force-displacement response of an SMA spring under: (a) Displacement-control loading and (b) Force-control loading.
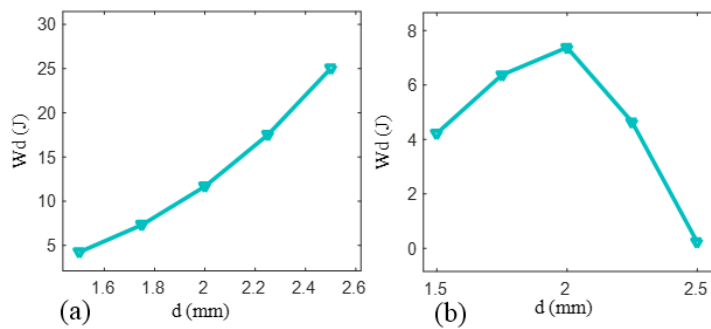

Fig. 10. The effect of wire diameter on energy dissipation under: (a) Displacement-control loading and (b) Force-control loading.
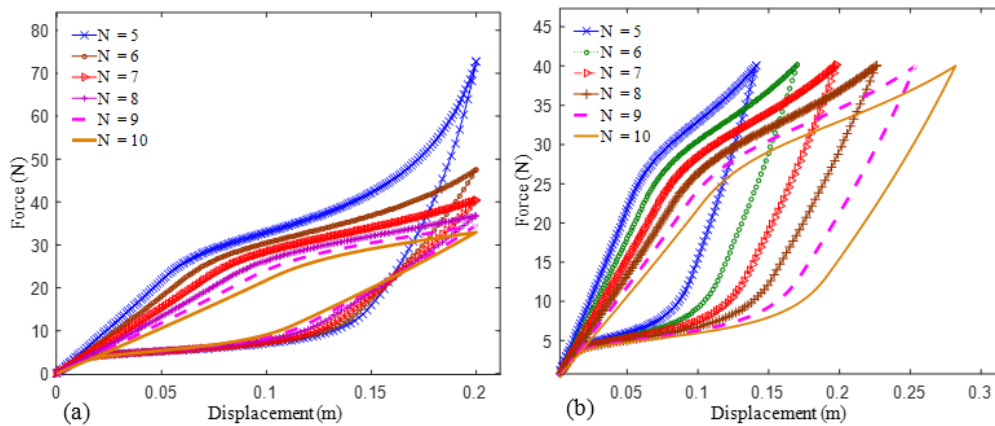

Fig. 11. The effect of number of active coils on force-displacement response of an SMA spring under: (a) Displacement-control loading and (b) Force-control loading.
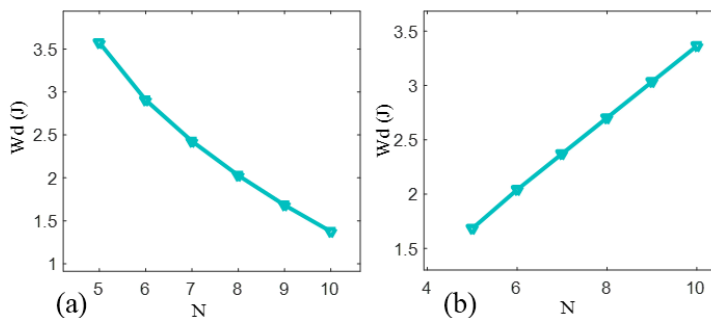

Fig. 12. The effect of number of active coils on energy dissipation under: (a) Displacement-control loading and (b) Force-control loading.
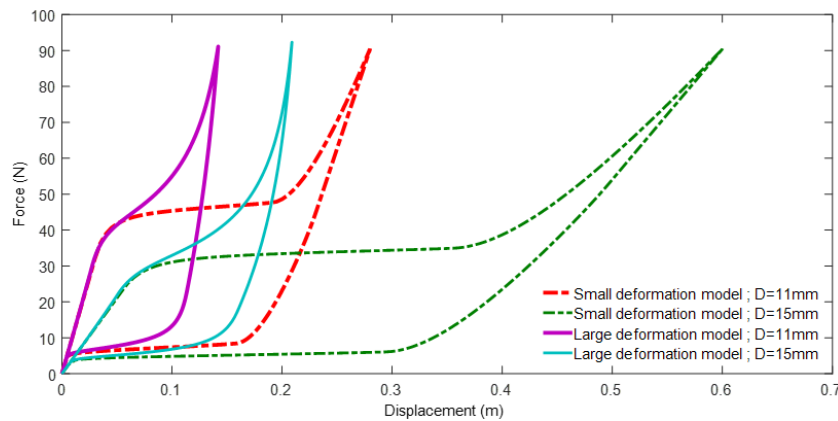
Fig. 13. Comparison between small and large deformation models for springs with 11mm and 15mm diameter.

Below is a framework for designing a pseudoelastic spring based on the presented figures:

- The first step is numerical implementation of the presented model using Eqs. (4-13) (whether under displacement- or force-control loadings). It is worth noting that performing numerical simulation employing presented model for displacement-control loadings is much easier than the force-control ones.

- A prototype SMA spring is needed which can be fabricated through a shape setting process as detailed in the experiment section.

- Material characterization and verification of numerical results can be conducted by using tensile or compressive tests on the fabricated samples.

- Then, a user should compare dissipative performance of the fabricated spring with the desired one in order to redesign the geometry if required. Figs. 7-12 provide a guideline according to operative conditions of an SMA spring. For the purpose of obtaining maximum dissipative performance under force-control loadings through change in the diameter of the spring and the wire, optimization of the geometry is needed. In fact, without calculations, the effects of these two parameters are not predictable.

- Finally, after redesigning the geometry, a user can fabricate a spring with the desired dissipative performance and employ the product in a suspension or isolator system.

Figs. 7b and 8b can be regenerated employing both large and small deformation models, and variations of dissipated energy with change in the spring diameter under a force-control condition can be compared. Fig. 13 compares the responses for 11mm and 15mm spring diameters. As shown in Fig. 14, neglecting the effects of large deformation can greatly change the trend of dissipative performance of an SMA spring.
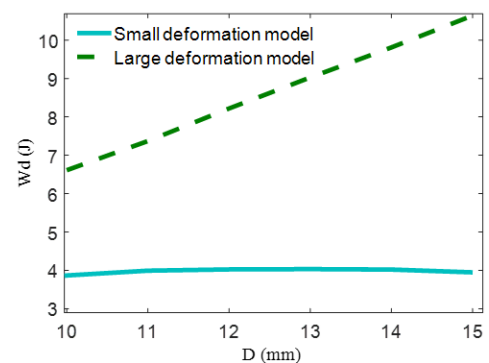

Fig. 14. Comparison between small and large deformation models in prediction of the dissipated energy.

5. Conclusions

In this work, considering geometric variations in the course of loading/unloading, an available model for SMA springs was generalized for springs undergoing large amounts of displacement. SMA springs exhibiting pseudoelastic response at the ambient temperature were fabricated from wire showing the same response at the room temperature. Some tensile tests were conducted on the fabricated springs, and the numerical results were shown to be in good agreement with experiment findings. Under small amounts of tensile displacement, the response of SMA spring can be predicted by small deformation model while, under large amounts of displacement, the usage of small deformation model may be accompanied by a remarkable error. Unlike tension, under compressive loadings, due to the effect of initial helix angle, employing large deformation model is required even at the initial stages of loading. The presented model is not limited to pseudoelastic response and it can also be employed to shape memory effect. Under displacement-control loadings, the dissipated energy declines with increasing D or N but increases with increasing d. Under force-control loadings, the dissipated energy increases by increasing N; however, an optimization process for D or d is needed. The significance of the geometry impact on

dissipated energy is that, in designing a superelastic SMA spring with optimized dissipative performance, the presented geometric study gives a designer a better vision and guideline for setting the geometrical param- eter. At last, it was shown that the geometric study will not be correct unless the large deformation model is employed.
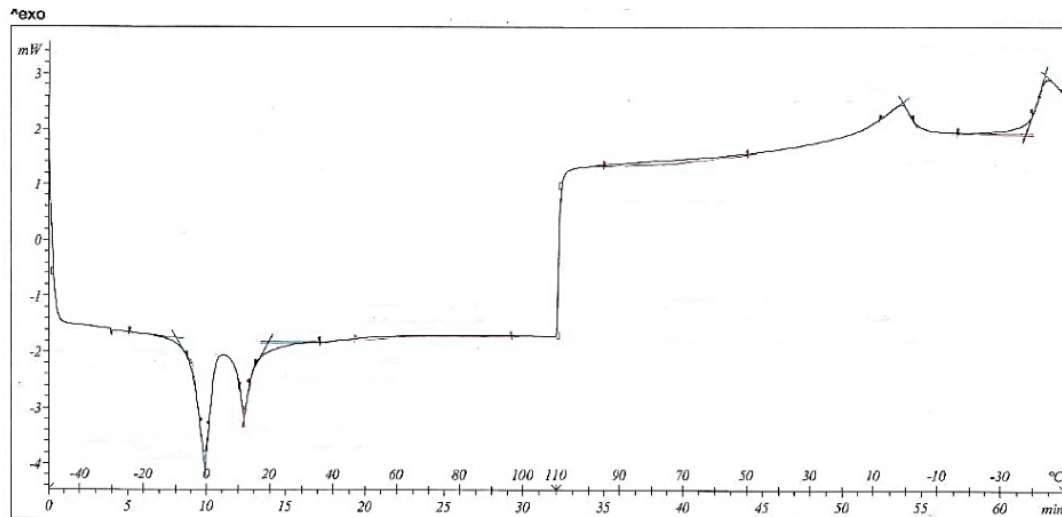
Appendix A

Fig. A.15. Results of DSC test for a fabricated spring.

References

[1] K. Yamauchi, I. Ohkata, K. Tsuchiya, S. Miyazaki, Shape memory and superelastic alloys: Applications and technologies, Elsevier, (2011).

[2] L. Janke, C. Czaderski, M. Motavalli, J. Ruth, Applications of shape memory alloys in civil engineering structures-overview, limits and new ideas, Mater. Struct., 38(5) (2005) 578-592.

[3] A. Saeedi, M.M. Shokrieh, Effect of shape memory alloy wires on the enhancement of fracture behavior of epoxy polymer, Polym. Test., 64 (2017) 221-228.

[4] S.W. Kim, J.G. Lee, S. An, M. Cho, K.J. Cho, A large-stroke shape memory alloy spring actuator using double-coil configuration, Smart Mater. Struct., 24(9) (2015) 095014.

[5] D. Patil, G. Song, A review of shape memory material's applications in the offshore oil and gas industry, Smart Mater. Struct., 26(9) (2017) 093002.

[6] P. Zhuang, S. Xue, P. Nie, W. Wang, Experimental and numerical study on hysteretic performance of SMA spring-friction bearings, Earthq. Eng. Eng. Vib., 15(4) (2016) 597-609.

[7] G. Attanasi, F. Auricchio, M. Urbano, Theoretical and experimental investigation on SMA superelas- tic springs, J. Mater. Eng. Perform., 20(4-5) (2011) 706-711.

[8] M.A. Savi, P.M.C. Pacheco, M.S. Garcia, R.A. Aguiar, L.F.G. de Souza, R.B. Da Hora, Nonlinear geometric influence on the mechanical behavior of shape memory alloy helical springs, Smart Mater. Struct., 24(3) (2015) 035012.

[9] J. Wang, Z. Moumni, W. Zhang, W. Zaki, A ther- momechanically coupled finite deformation consti- tutive model for shape memory alloys based on Hencky strain, Int. J. Eng. Sci., 117 (2017) 51-77.

[10] S.M. An, J. Ryu, M. Cho, K.J. Cho, Engineer- ing design framework for a shape memory alloy coil spring actuator using a static two-state model, Smart Mater. Struct., 21(5) (2012) 055009.

[11] S. Enemark, I.F. Santos, M.A. Savi, Modelling, characterisation and uncertainties of stabilised pseudoelastic shape memory alloy helical springs, J. Intell. Mater. Syst. Struct., 27(20) (2016) 2721- 2743.

[12] M.M. Khan, D.C. Lagoudas, Modeling of shape memory alloy pseudoelastic spring elements us- ing Preisach model for passive vibration isolation, Smart Mater. Struct., 4693 (2002) 336-348.

[13] B. Heidari, M. Kadkhodaei, M. Barati, F. Karimzadeh, Fabrication and modeling of shape memory alloy springs, Smart Mater. Struct., 25(12) (2016) 125003.

[14] F. Jahanbazi, Experimental and Theoretical Study of Superelastic Shape Memory Alloy Coil

Springs, Master Thesis, Isfahan University of Technology, (2017).

[15] L.C. Brinson, One-dimensional constitutive behavior of shape memory alloys: thermomechanical derivation with non-constant material functions and redefined martensite internal variable, J. Intell. Mater. Syst. Struct., 4(2) (1993) 229-242.

[16] J.H. Chung, J.S. Heo, J.J. Lee, Implementation strategy for the dual transformation region in the Brinson SMA constitutive model, Smart Mater. Struct., 16(1) (2006) N1-N5.

[17] A.M. Wahl, Mechanical springs, Penton Publishing Company, (1944).

[18] S. Sameallah, M. Kadkhodaei, V. Legrand, L. Saint-Sulpice, S.A. Chirani, Direct numerical determination of stabilized dissipated energy of shape memory alloys under cyclic tensile loadings, J. Intell. Mater. Syst. Struct., 26(16) (2015) 2137-2150.

[19] M. Hesami, L. Pino, L. Saint-Sulpice, V. Legrand, M. Kadkhodaei, S. Arbab Chirani, S. Calloch, Rotary bending fatigue analysis of shape memory alloys, J. Intell. Mater. Syst. Struct., c29(6) (2018) 1183-1195.